Combined Prospective Rigid-Body Motion Correction with Retrospective Non-Rigid Distortion Correction for EPI

M. B. Ooi[1], R. Bammer[1], and T. R. Brown[2]

[1]Radiology, Stanford University, Stanford, CA, United States, [2]Radiology, Medical University of South Carolina, Charleston, SC, United States

Introduction: Prospective real-time motion correction, where the scan-plane orientation is dynamically updated to track with the subject's head during an MRI scan, is becoming increasingly popular (1-7). While these methods focus on compensating for bulk rigid-body motion, a secondary effect of head motion is non-rigid-body image distortion caused by changes in the effective shim within the brain. These changes occur as the brain's orientation changes relative to the B_0 field (8), and cannot be compensated for with a rigid-body model. Echo-planar imaging (EPI) is particularly sensitive to field inhomogeneities due to its low phase-encode bandwidth. If the head moves during an EPI time-series scan (e.g. fMRI, DTI, PWI), even after adaptive rigid-body realignment, a residual non-rigid warping of the brain will remain in the phase-encode direction (9), which can increase signal fluctuation and impair the veracity of data. We propose an approach that uses prospective motion correction in combination with retrospective distortion correction to obtain images that are compensated for both rigid motions and susceptibility-induced non-rigid deformations.

Methods: Experiments were performed on a 1.5T Philips Achieva (Philips Medical Systems, Best, The Netherlands) with a standard bird-cage coil. Prospective rigid-body motion correction was established using radio-frequency micro-coils, or "active markers", in a setup as detailed in (5,10). Slice-by-slice prospective correction was applied to an axial, single-shot 2D-EPI time-series (TE/TR = 40/1680 ms, θ = 85º, FOV = 192×192 mm, matrix = 64×64 mm, thickness/gap = 5/1 mm, slices = 20, time-frames = 10). Scans were performed on a volunteer trained to reproduce two types of motion: a continuous left-right "head-shake" rotation of ~ ±5º, and a continuous head-foot "head-nodding" rotation of ~ ±5º. Left-right and head-foot rotations induce in-plane and through-plane motions, respectively, and were designed to investigate the relationship between head orientation and shim changes within the brain.

Complex EPI-data from the prospectively corrected images was saved to generate field-maps for additional retrospective distortion correction. Phase images $\mathbf{\Phi}_n$ of the n^{th} time-frame were unwrapped (11), and the field variation map $\Delta\mathbf{B}_n$ calculated: $\Delta\mathbf{B}_n = (\mathbf{\Phi}_n - \mathbf{\Phi}_1)/(2\pi\text{TE})$. $\Delta\mathbf{B}_n$ thus yields a frequency-difference map (Hz) of the relative field inhomogeneity deviation between the n^{th} and first (reference) time-frame due to the different head positions. Since field inhomogeneities cause negligible pixel mis-location in the readout direction for EPI, the distortion correction then simplifies into a series of 1D pixel-shifts in the phase-encode direction which – due to the prospective scan-plane tracking – remains "locked" to the patient orientation. To calculate the necessary pixel-shifts, the local $\Delta\mathbf{B}_n$ is converted into a pixel-shift map $\mathbf{r}_n = \Delta\mathbf{B}_n/BW_{pe}$, where BW_{pe} is the bandwidth per pixel (~ 20 Hz/pixel) in the phase-encode direction. A shifting algorithm (9) was implemented where the value of each pixel at location $\mathbf{r}_n$ was used to shift the corresponding image pixel in the phase-encode direction. In this manner every n^{th} time-frame was undistorted back to the reference. This (non-rigid-body) distortion correction was retrospectively applied to the (rigid-body) prospectively corrected dataset.

To quantify improvement in image stability, the standard deviation (σ) of each pixel's image intensity was calculated over the time series. As movement increases the intensity variation of each pixel, the result of perfect motion correction will be to reduce σ back to levels when the subject remained still.

Results: Figure 1 shows a scatter-plot with each point representing a single slice, where the maximum frequency variation across the slice (measured from $\Delta\mathbf{B}_n$) is plotted as a function of rotational displacement (measured from the active marker positions, relative to the first time-frame). As rotation increases, frequency variation across each slice also increases, with the rate of increase ~ 3 times greater for through-plane (θ_{tp}) vs. in-plane (θ_{ip}) rotations. Exemplary field maps measured near the maximum in-plane (θ_{ip} = 4.25°) and through-plane (θ_{tp} = 5.54°) rotations performed by the volunteer are shown in Fig. 1b and 1c, respectively. For the in-plane case (Fig. 1b), frequency-shifts did not exceed 4 Hz (or a pixel-shift = 0.6 mm), while in the through-plane case (Fig. 1c) shifts of 20 Hz (3 mm) were observed.

Figure 2 shows a slice acquired during through-plane motion with phase-encoding in the left/right (L/R) direction. The difference images in Fig. 2b-d were generated by subtracting the reference slice (Fig. 2a) from the slice acquired at θ_{tp} = 5.54°. A zero difference image represents perfectly realigned time-frames. Despite substantial improvement over the uncorrected case (Fig. 2b), residual error remains in the prospectively corrected image (Fig. 2c), emphasized by white/black arrows that denote areas of positive/negative difference, respectively – this indicates an uncorrected non-rigid shear in the L/R phase-encode direction, and is consistent with the regions of increased frequency variation in the corresponding field map (Fig. 1c). Prospective correction followed by retrospective distortion-correction (Fig. 2d) using the field map in Fig. 1c reduces this shear-like artifact, yielding a near-zero difference image. This improved image stability is confirmed by an average reduction of 13% in σ (between prospective + distortion correction vs. prospective correction alone) over all brain pixels, with an average reduction of 31% in an ROI in the anterior region where the distortion was most severe. For the case of in-plane motion (images not shown), prospective correction alone resulted in near-perfect correction, with additional retrospective distortion correction improving σ only marginally (~ 2%); this is consistent with the minimal frequency-shifts seen in Fig. 1a,b and common wisdom that head-nodding relative to B_0 is predominantly responsible for susceptibility gradient variations.

Fig. 1

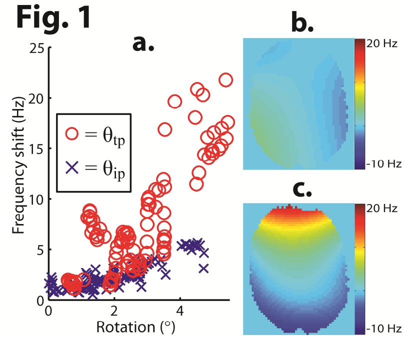

Fig. 2

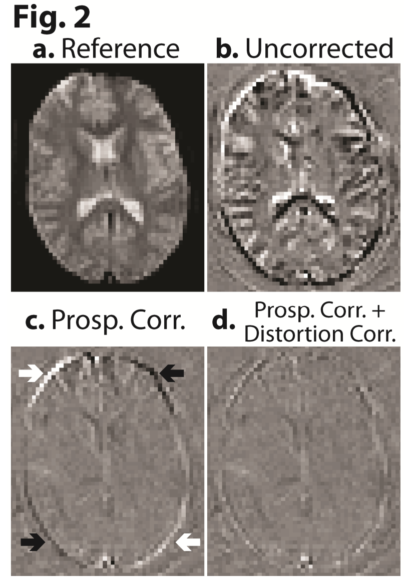

Discussion & Conclusion: Non-rigid-body image-distortion due to motion-induced B_0 variations is a remaining source of signal variance that can be reduced using an appropriate unwarping algorithm. Image stability was further improved (i.e. σ reduced) when prospective rigid-body correction was followed by retrospective distortion-correction using the phase differences between time-frames. While other retrospective motion and distortion correction schemes face the challenge that distortions will be in different directions (dependent on the current orientation of the head relative to the initially prescribed phase-encode direction), this approach only has to deal with distortions along one dimension since the phase-encode direction prospectively tracks with the head orientation. Moreover, while other unwarping methods are based on field maps prediction (12) and/or require a susceptibility model of the imaged object (13), the presented method uses the measured phase information and requires only that the complex EPI-data is saved.

Note that this distortion correction method only corrects for time-varying field inhomogeneities, as unwarping is performed relative to the first time-frame. To compensate for static inhomogeneities still present in all time-frames (i.e. unwarp to the "true geometry"), one more stage of unwarping may be performed on the time-series by using a single EPI-volume acquired with a different TE (9). The improved image stability demonstrated here will potentially benefit the detection-sensitivity of task activation in fMRI as well as perfusion and diffusion MRI.

Grant funding: NIH R21EB006877, NIH/NCRR UL1RR024156, NIH 5R21EB006860-02, NIH 1R01EB011654-01

References: [1] van der Kouwe AJW et al., MRM 2006;56(5):1019-32. [2] Zaitsev M et al., Neuroimage 2006;31(3):1038-50. [3] Aksoy M et al., ISMRM 2008;3120. [4] Qin L et al., MRM 2009;62(4):924-34. [5] Ooi MB et al.,MRM 2009;62(4):943-54. [6] Thesen S et al., MRM 2000;44(3):457-65. [7] White N et al.,MRM 2010;63(1):91-105. [8] Jezzard P et al., HBM 1999;8(2-3):80-85. [9] Jezzard P et al., MRM 1995;34(1):65-73. [10] Ooi MB et al., ISMRM 2010;5038. [11] Jenkinson M, MRM 2003;49(1):193-97. [12] Andersson JL et al., Neuroimage 2001;13(5):903-19. [13] Boegle R et al., MAGMA 2010;23(4):263-73.